Available online at www.sciencedirect.com
SCIENCE DIRECT
Biochimica et Biophysica Acta 1715 (2005) 81 – 95
BIOCHIMICA ET BIOPHYSICA ACTA
BBA
http://www.elsevier.com/locate/bba

Structure and orientation study of fusion peptide FP23 of gp41 from HIV-1 alone or inserted into various lipid membrane models (mono-, bi- and multibi-layers) by FT-IR spectroscopies and Brewster angle microscopy

Sabine Castano*, Bernard Desbat

Laboratoire de Physico-Chimie Moléculaire (LPCM), UMR CNRS 5803, Université de Bordeaux I, 351 cours de la Libération, 33405 Talence, France

Received 10 March 2005; received in revised form 12 July 2005; accepted 19 July 2005
Available online 8 August 2005

Abstract

In the present work, we study the structure and the orientation of the 23 N-terminal peptide of the HIV-1 gp 41 protein (AVGIGALFLGFLGAAGSTMGARS) called FP23. The behaviour of FP23 was investigated alone at the air/water interface and inserted into various lipid model systems: in monolayer or multibilayers of a DOPC/cholesterol/DOPE/DOPG (6/5/3/2) and in a DMPC bilayer. PMIRRAS and polarized ATR spectroscopy coupled with Brewster angle microscopy and spectral simulations were used to precisely determine the structure and the orientation of the peptide in its environment as well as the lipid perturbations induced by the FP23 insertion. The infra-red results show the structural polymorphism of the FP23 and its ability to transit quasi irreversibly from an α-helix to antiparallel β-sheets. At the air/water interface, the transition is induced by compression of the peptide alone and is modulated by compression and lipid to peptide ratio (Ri) when FP23 is inserted into a lipid monolayer. In multibilayers and in a single bilayer, there is coexistence in quasi equal proportions of α-helix and antiparallel β-sheets of FP23 at low peptide content (Ri=100, 200) while antiparallel β-sheets are predominant at high FP23 concentration (Ri=50). In (multi)bilayer systems, evaluation of dichroic ratios and sprectral simulations show that both the α-helix and the antiparallel β-sheets are tilted at diluted FP23 concentrations (tilt angle of α-helix with respect to the normal of the interface=36.5±3.0° for FP23 in multibilayers of DOPC/Chol/DOPE/DOPG at Ri=200 and 39.0±5.0° in a single bilayer of DMPC at Ri=100 and tilt angle of the β-sheets=36.0±2.0° for the β-sheets in multibilayers and 30.0±2.0° in the lipid bilayer). In parallel, the FP23 induces an increase of the lipid chain disorder which shows both by an increase of the methylene stretching frequencies and an increase of the average C–C–C angle of the acyl chains. At high FP23 content (Ri=50), the antiparallel β-sheets induce a complete disorganization of the lipid chains in (multi)bilayers.

Keywords: Fusion peptide FP23; Lipid-bound structure; Peptide orientation; PMIRRAS; ATR spectroscopy; Brewster angle microscopy

1. Introduction

Fusion between the membranes of enveloped viruses such as immunodeficiency virus type I (HIV-1) and the membrane of the target host cells is an essential step in infection [1–5]. For HIV-1 virus, this process is mediated by the integral membrane viral envelope gp41 protein that contains a N-terminal apolar segment generally referred as the fusion domain or fusion peptide (FP) [6]. Strong evidence coming from mutagenesis studies of intact

Abbreviations: DMPC, dimirystoyl-phosphatidylcholine; DOPC, dioleyl-phosphatidylcholine; DOPG, dioleyl-phosphatidylglycerol; DOPE, dioleyl-phosphatidylethanolamine; PMIRRAS, polarization modulation infra-red reflection absorption spectroscopy; ATR, attenuated total reflexion spectroscopy; BAM, Brewster angle microscopy

* Corresponding author. Tel.: +33 5 40 00 63 64; fax: +33 5 40 00 66 45.
E-mail address: s.castano@lpcm.u-bordeaux1.fr (S. Castano).

0005-2736/$ - see front matter © 2005 Elsevier B.V. All rights reserved.
doi:10.1016/j.bbamem.2005.07.008

enveloped proteins as well as from synthetic FPs implicates the role of the FP domain in membrane fusion. Indeed, this FP domain displays many membrane perturbing properties, causes fusion of liposomes and erythrocytes and strong correlations have been shown between fusion peptide-induced liposome fusion and viral/host cell fusion [7–22]. Therefore, the FP peptide seems to be a useful model to understand the mechanism of fusion.

To solve the structure of FP and correlate with its putative function, numerous experimental techniques (CD, solid and solution NMR, fluorescence, ESR, IR) have been used in mimetic membrane environments but they have yielded complex and sometimes contradictory results.

For instance, CD measurements on the FP domain show significant α-helical character for samples in organic solvent [19,23–25], in SDS detergent at a 1/200 peptide/lipid ratio [19,23,26] and in environment of negatively charged POPG vesicles with 1/200 peptide/lipid mole ratio [9]. Some NMR studies on the peptide in SDS, or DPC (peptide/lipid ratio 1/45) and DPC/SDS (4/1) micelles are also consistent with a helical central region [24,27] but other solid state NMR studies have shown that the FP peptide adopts an oligomeric β-strand structure when associated with a lipid and cholesterol mixture which composition is close to that of the membrane host cells of the virus either at high peptide/lipid ratio (1/20) or in the peptide/lipid ratio 1/200 to 1/20 [28–31]. In contrast, other NMR and EPR studies show a conformational change from α-helix to β-sheet in EPC SUV vesicles when the peptide/lipid ratio decreases from 200 to 25 [32].

When infra-red (IR) spectroscopy is used, the same contradictory results are obtained. Indeed, with neutral lipid vesicles or erythrocytes ghosts at peptide/lipid ratios of 1/200, some authors report predominantly helical structure [12,23], others predominantly β-structure [9,20,33] and mixed helical and β-structure [11]. Some investigators show that in neutral lipids the peptide conformation changes from helix to β-sheet as the peptide/lipid ratio is increased from 1/200 to 1/30 [12,23] while others report that the β conformation does not change with these ratios [9,20]. Some authors demonstrate that the FP conformation varies with the peptide/lipid ratio in presence of negatively charged lipids (POPG or POPG/POPC vesicles) and evolves from α-helix to β-sheet when the peptide/lipid ratio is increased from 1/200 to 1/30 or 1/75 to 1/10, respectively [9,34]. These differences in structures may have to do with differences in peptide sequence, lipid composition, sample preparation, hydration level and also solvent used to solubilize the peptide. Indeed, highly hydrophobic dimethyl sulfoxide (DMSO) was often used to solubilize FP peptides [9,11–13,19,20,32,33,35] but is very difficult to eliminate from membrane interface during peptide interactions. Therefore, DMSO may strongly influence the FP's behaviour unlike solvent such as hexafluoroisopropanol which is more polar and then easier to remove from membrane interface.

In the present work, to try to clarify the previously obtained results, we carefully investigate the structure and the orientation of the FP domain corresponding to the 23 N-terminal residues of the HIV-1 gp 41 protein (AVGIGALFLGFLGAAGSTMGARS), called FP23, using several IR spectroscopy techniques: PMIRRAS at the air/water interface of the peptide alone and inserted into lipid monolayers and ATR spectroscopy of peptide inserted in bi- and multibi-layers. The investigations at the air/water interface were combined with Brewster angle microscopy to analyze the morphology of the pure FP23 and mixed FP23/lipid monolayers. The orientational IR experimental results were analyzed using home-developed spectral simulation programs.

2. Materials and methods

2.1. FP23 and lipids

Synthetic peptide FP23 (AVGIGALFLGFLGAAGSTMGARS-NH_2) was purchased from Bachem (Bubendorf, Switzerland). It is free at the N-term and amidated at the C-term. FP23 was solubilized in hexafluoroisopropanol (HFIP) from Sigma at micromolar concentrations. Lipids (DOPC, DMPC, DOPE, DOPG, cholesterol) were from Sigma. A phosphate buffer (60 mM, NaCl 100 mM, pH = 7.4) either in H_2O or in D_2O was used for all the experiments.

2.2. Film formation and surface pressure measurements

Monolayer experiments were performed on a computer-controlled Langmuir film balance (Nima Technology, Coventry, England). The rectangular trough (V = 110 cm^3, S = 145 cm^2) and the barrier were made of Teflon. The surface pressure (Π) was measured by the Wilhelmy method using a filter paper plate. The trough was filled with the aqueous phosphate buffer using ultra pure water (Milli-Q, Millipore). The experiments were carried out at 25 ± 2 °C.

Pure FP23 films were obtained by deposition of few μl of HFIP peptide stock solutions at the air/water interface to define the total peptide concentration. Mixed peptide/lipid films were obtained by codeposition of FP23/lipid mixture at the surface at the defined lipid to peptide ratio, Ri. The monolayer lipid composition used was DOPC/cholesterol/DOPE/DOPG 6/5/3/2. Then, after ≈15 min the mixed lipid/peptide film was slowly compressed up to 30 mN/m.

2.3. PMIRRAS spectroscopy

PMIRRAS spectra were recorded on a Nicolet Nexus 870 spectrometer equipped with a photovoltaic HgCdTe detector cooled at 77 K. Generally, 200 or 300 scans were coadded at a resolution of 4 cm^{-1} or 8 cm^{-1} for pure peptide or mixed peptide/DMPC monolayers respectively. In short, PMIRRAS combines FT-IR reflection spectroscopy with fast polarization modulation of the incident beam between parallel (p) and perpendicular (s) polarization. Two-channel processing of the detected signal makes it possible to obtain the differential reflectivity spectrum:

$$\Delta R/R = (\mathrm{Rp} - \mathrm{Rs})/(\mathrm{Rp} + \mathrm{Rs})J_2.$$

To remove the contribution of liquid water absorption and the dependence on Bessel functions J_2, the monolayer spectra are divided by that of the subphase. With an incidence angle of 75°, transition moments preferentially oriented in the plane of the interface give intense and upward oriented bands, while perpendicular ones give weaker and downward oriented bands [36].

The decomposition of the amide I and amide II spectral region (1500–1800 cm^{-1}) into individual bands was performed with the Peaksolve (version 3.0, Galactic) software and analyzed as a sum of Gaussian/Lorentzian curves, with consecutive optimization of amplitudes, band positions, half-width and Gaussian/Lorentzian composition of the individual bands.

2.4. ATR spectroscopy of bilayers and multibilayers

The pure DMPC or mixed FP23/DMPC bilayers adsorbed on a germanium ATR crystal were obtained by spontaneous fusion of small unilamellar vesicles (SUV) of pure DMPC or mixed FP23/DMPC. SUV were prepared by tip sonication for ≈30 min after direct hydration by D_2O buffer of the lipid powder. For mixed FP23/DMPC bilayer, SUV were prepared by hydration of a film obtained after evaporation from a mixture at a defined Ri of DMPC in $CHCl_3$ and FP23 in HFIP. After bilayer formation a the crystal surface, the excess of SUV was replaced by a buffer solution in D_2O. The single bilayer formation was controlled both by the measurement of the absolute IR intensity and by measurement of the thickness using ellipsometry (not shown).

Multibilayers were obtained by shearing a pure lipid or mixed FP23/lipid gel at the diamond ATR crystal surface (golden gate, Eurolabo, France). The gel was obtained by rehydration of the pure lipid mixture or FP23/lipid mixture with D_2O buffer after solvent evaporation. Hydration ratios were higher than 70%.

ATR spectra were recorded either on a Nicolet Magna 550 spectrometer equipped with a MCT detector cooled at 77 K or on a Nicolet Nexus 670 spectrometer equipped with a DTGS detector. Since ATR spectroscopy is sensitive to the orientation of the structures [37–39], spectra were recorded with a parallel (p) and perpendicular (s) polarization of the incident light with respect to the ATR plate. Generally 1000 scans were coadded at a resolution of 8 cm^{-1} and a two-level zero filling. All the orientational information is then contained in the dichroic ratio $R_{ATR} = Ap/As$, where Ai represents the absorbance of the considered band for the p or s polarization of the incident light, respectively.

2.5. Simulation of the amide I region of ATR spectra for α-helix and β-sheets inserted in bilayers and multibilayers: determination of secondary structure orientations

Since ATR spectroscopy is very sensitive to the variations of the anisotropic indexes, it was interesting to evaluate precisely the orientation of the FP23 in the lipid systems taking into account the real electric fields interacting with the sample at the crystal interface. Therefore, we have performed simulations in which the oriented systems (α-helix and β-sheets) are dispersed in lipid layers.

To evaluate the anisotropic optical constants of ultrathin films in the space coordinate system, we have used a calculation procedure which allows a direct determination of the refractive indexes from experimental FTIR spectra [40]. Briefly, in this procedure, the in-plane (X and Y) and the out of plane (Z) refractive indexes are obtained from polarized normalized transmittance spectra at normal incidence and a p-polarized reflectance spectrum at grazing incidence (IRRAS), respectively.

The IR spectra from anisotropic optical constants were simulated using a computer program based on Abelès' matricial formalism developed in the laboratory and described elsewhere [40,41].

2.5.1. Determination of anisotropic optical constants of α-helix and antiparallel β-sheet for each orientation

The extinction coefficients for each orientation of the secondary structure were calculated in the space coordinate system (X, Y, Z) using the following general rotation matrix:

$$\begin{pmatrix} M_X \\ M_Y \\ M_Z \end{pmatrix} = \begin{pmatrix} \cos\Psi\cos\varphi - \cos\theta\sin\varphi\sin\Psi & -\sin\Psi\cos\varphi - \cos\theta\sin\varphi\cos\Psi & \sin\theta\sin\varphi \\ \cos\Psi\sin\varphi + \cos\theta\cos\varphi\sin\Psi & -\sin\Psi\sin\varphi + \cos\theta\cos\varphi\cos\Psi & -\sin\theta\cos\varphi \\ \sin\theta\sin\Psi & \sin\theta\cos\Psi & \cos\theta \end{pmatrix} \begin{pmatrix} \mathrm{Mu} \\ \mathrm{Mv} \\ \mathrm{Mw} \end{pmatrix}$$

which relates the components of the transition dipole moment vector $\boldsymbol{M}$ in the space and the molecular coordinate systems (u, v, w) [42]. The elements of the matrix represent the direction cosines expressed in term of the Euler angles ϕ (azimuthal angle, rotation around Z), θ (tilt angle, rotation around u) and Ψ (twist angle, rotation around w) [42]. Considering that the extinction coefficients are proportional to the square of the transition dipole moments, we obtain the relationships between the extinction coefficients in the two coordinate systems.

2.5.1.1. α-helix. The IR absorption of the amide I mode of the α-helix around 1655 cm^{-1} was described as a main transition moment parallel to the w axis and two components being perpendicular to the helix axis (u, v) [43,44]. Due to the uniaxial symmetry of the helical chain, the u and v directions of the transition moment cannot be distinguished. The maximal extinction coefficients values previously determined for poly-γ-benzyl-L-glutamate (PBG) were used to simulate the α-helix [45], they were adjusted to the experimental band width at half intensity considering that the total integrated intensity is conserved. Therefore, in the case of the α-helix of FP23, we used $k_u = k_v = 0.175$, $k_w = 0.30$ and $\Delta\nu_{1/2} = 30$ cm^{-1}. An initial position of the α-helix in the lipid layer plane (X, Y) was defined with the α-helix axis perpendicular to the lipid plane (Scheme I-A), which

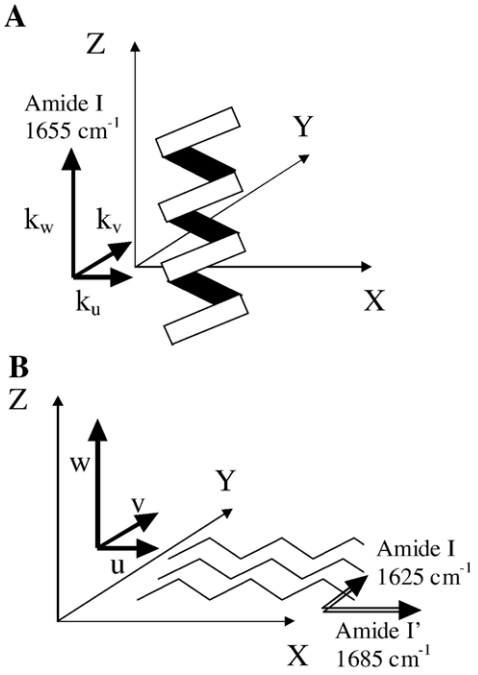

Scheme I. Schematic representation in the coordinate systems of the initial positions, A: of the α-helix; B: of the β-sheet.

means that (X, Y, Z) and (u, v, w) coordinate systems are overlapped. Rotation of the α-helix around its main axis in the lipid plane (X, Y) can be defined by varying the tilt angle θ ($\Phi = 0$ and $\Psi = 0$). The anisotropic extinction coefficients k_{aX}, k_{aY}, k_{aZ} for each angle θ in the space coordinate system can then be obtained using the following rotation matrix.

$$\begin{pmatrix} k_{aX} \\ k_{aY} \\ k_{aZ} \end{pmatrix} = \begin{pmatrix} 1 & 0 & 0 \\ 0 & \cos^2\theta & \sin^2\theta \\ 0 & \sin^2\theta & \cos^2\theta \end{pmatrix} \begin{pmatrix} ku \\ kv \\ kw \end{pmatrix}$$

Considering the uniaxial symmetry of the layer system, k_X and k_Y have to be averaged, $k_X = k_Y = k_{XY} = (k_{aX} + k_{aX})/2$. Then, for each angle θ of orientation, a set of extinction coefficients $(k_{XY}, k_Z)_\theta$ was calculated and an anisotropic indexes file for each orientation of the α-helix was generated.

2.5.1.2. Antiparallel β-sheet. Due to the two dimensional symmetry and the selection rule of an antiparallel β-sheet [44,46,47], the IR absorption modes were described with an amide I vibration around 1625 cm^{-1} corresponding to the interchain hydrogen bonds (along v axis) and an amide I′ vibration around 1685 cm^{-1} oriented along the β-sheet axis (along u axis) (Scheme I-B). The maximal extinction coefficients values previously determined for the model peptide $K(LK)_7$ containing lysine (K) and leucine (L) residues were used to simulate the β-sheet [45]. As previously described, the extinction coefficients were adjusted to the experimental band width at half intensity considering that the total integrated intensity is conserved, then k_v(1625 cm^{-1}) = 1.6 ($\Delta\nu_{1/2}$ = 15 cm^{-1}) and k_u (1685 cm^{-1}) = 0.25 ($\Delta\nu_{1/2}$ = 8 cm^{-1}) were used for the β-sheet of

FP23. An initial position of the β-sheet in the lipid layer plane (X, Y) was defined when the β-sheet is flat oriented in the lipid plane (Scheme I-B), which means that the (X, Y, Z) and (u, v, w) coordinate systems are overlapped. Rotations of the β-sheet in the lipid plane (X, Y) can be defined by varying the tilt angle θ (rotation around u) and the twist angle Ψ (rotation around w) with $\Phi = 0$. The anisotropic extinction coefficients k_{aX}, k_{aY}, k_{aZ} in the space coordinate system for each combination of angles (θ, Ψ) can then be obtained for the amide I (1625 cm^{-1}) and amide I' (1685 cm^{-1}) mode using the following rotation matrix:

$$\begin{pmatrix} k_{aX} \\ k_{aY} \\ k_{aZ} \end{pmatrix} = \begin{pmatrix} \cos^2\Psi & \sin^2\Psi & 0 \\ \cos^2\theta\sin^2\Psi & \cos^2\theta\cos^2\Psi & \sin^2\theta \\ \sin^2\theta\sin^2\Psi & \sin^2\theta\cos^2\Psi & \cos^2\theta \end{pmatrix} \begin{pmatrix} ku \\ kv \\ kw \end{pmatrix}$$

Considering the uniaxial symmetry of the layer system, k_X and k_Y have to be averaged, then $k_X = k_Y = k_{XY} = (k_{aX} + k_{aY})/2$. For each ($\theta$, Ψ) combination a set of extinction coefficients $(k_{XY}, k_Z)_{1625}$ and $(k_{XY}, k_Z)_{1685}$ was calculated and an anisotropic indexes file for each orientation of the β-sheet was generated. Due to the lack of revolution symmetry of a β-sheet, numerous (θ, Ψ) combinations are possible. Therefore, only the calculations corresponding to the ones close to the experimental data will be presented in Results.

2.5.2. Simulation of the polarized ATR spectra of α-helix and β-sheet inserted in lipid layers (bi- or multi-)

Using the calculation procedure described previously [40], the anisotropic optical constants determined for DOPC layers (paper in preparation) were used to simulate the lipid matrix. The extinction coefficients determined for the C═O ester stretching mode around 1735 cm^{-1} (ν(C═O)) and the CH_2 bending mode around 1480 cm^{-1} ($\delta(CH_2)$) were used to generate an anisotropic indexes file of the lipid. This file was mixed in a fixed massic peptide/lipid ratio with each extinction coefficients file of the α-helix or the β-sheet corresponding to one orientation of the secondary structure in the lipid matrix.

The p-polarized and s-polarized ATR spectra of bi- or multi-bilayers on germanium ($n = 4$) and diamond ($n = 2.4$), respectively, were then simulated using each file of anisotropic optical constants obtained [40]. For each orientation, it was possible to extract the dichroic ratio, R_{ATR}, of the amide I band at 1655 cm^{-1} of the α-helix, and the amide I band at 1625 cm^{-1} and amide I′ band at 1685 cm^{-1} of the β-sheet. These ratios were then compared with the experimental ones in order to determine the orientations of the secondary structures in the bi- or multibi-layers.

2.6. Brewster angle microscopy (BAM) measurements

The morphology of pure FP23 or mixed FP23/lipid layers at the air/water interface were observed using a Brewster angle microscope (NFT BAM*2plus*, Göttingen, Germany) mounted on the Langmuir trough. The microscope was equipped with a frequency doubled Nd:Yag laser (532 nm, 50 mW), polarizer, analyser and a CCD camera. The spatial resolution of the BAM was about 2 μm, and the image size 625 × 400 μm with ×10 lens used.

3. Results

3.1. PMIRRAS and BAM study of the FP23 at the air/water interface

3.1.1. FP23 alone at the air/water interface

The in-situ PM-IRRAS spectra at the air/water interface of a FP23 film during compression from 1 to 30 mN/m display well resolved amide I bands between 1600 and 1700 cm^{-1} and a broad amide II band centered around 1530 cm^{-1} (Fig. 1A). The amide I domain evolves during the compression. At low surface pressure (1 mN/m), the amide I band is centered around 1655 cm^{-1} with shoulders around 1620 cm^{-1} and 1690 cm^{-1}, which correspond respectively to α-helix and antiparallel β-sheets [38,44,48,49]. When the lateral pressure increases from 5 to 30 mN/m main amide I contributions around 1655 cm^{-1} and 1625 cm^{-1} increase due to the higher density of FP23 under the IR beam, but the band around 1625 cm^{-1} progressively becomes predominant. At 30 mN/m, the main amide I band is centered around 1627 cm^{-1} with a shoulder around 1655 cm^{-1}. Such a change is characteristic of a progressive structural transition from an α-helix to antiparallel β-sheets induced by the lateral pressure increase. In parallel to pressure increase, there is also a progressive increase of the maximal frequency of the amide I band of the β-sheet from 1621 cm^{-1} to 1627 cm^{-1}. Such a modification is characteristic of a progressive weakening and distorsion of the hydrogen bonds when the β-sheets become more constrain and more subject to steric hindrance at the interface. At 1 mN/m, the amide I (1655 cm^{-1})/amide II (1530 cm^{-1}) ratio ≈2.3 indicates that the helix axis is tilted from approximately 60° with the normal to the interface plane [50,51]. At 30 mN/m, the strong amide I (1625 cm^{-1})/amide I′ (1690 cm^{-1}) ratio indicates that the β-sheets are mainly flat oriented in the interface plane [50–52].

During decompression from 30 mN/m to 1 mN/m (Fig. 1B), there is an intensity decrease due to the progressive lowering of FP23 surface concentration in the IR beam but no change in the form of the amide I domain. The main amide I band remains centered around 1627 cm^{-1} (and amide I′ around 1690 cm^{-1}) with a shoulder around 1655

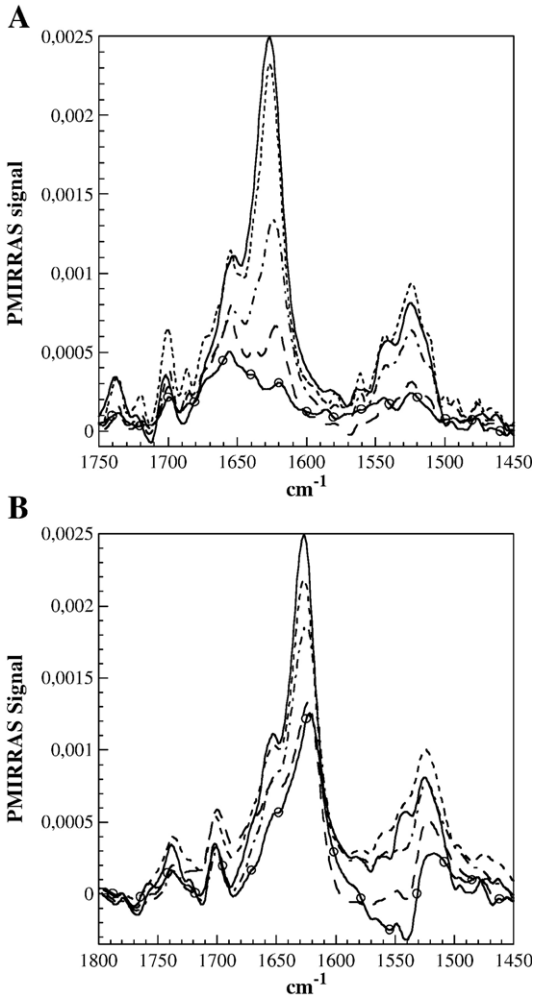

Fig. 1. PM-IRRAS spectra of FP23 alone at the air/water interface. A: During compression —○— 1 mN/m; – – – 5 mN/m; –·–·– 10 mN/m, - - - 20 mN/m, —— 30 mN/m. B: During decompression —○— 1 mN/m; – – – 5 mN/m; –·–·– 10 mN/m, - - - 20 mN/m, —— 30 mN/m. Subphase: phosphate buffer 60 mM, NaCl 100 mM, pH=7.5–T=23 °C.

cm^{-1} which means that the antiparallel β-sheet structure remains predominant with a small amount of α-helix even at low surface pressure. This experiment shows the quasi irreversibility of the structure transition from α-helix to antiparallel β-sheets observed during the compression (or at least the slow kinetics of reverse transition at the time scale of observation): antiparallel β-sheets remain the predominant secondary structure of FP23 at low surface pressure after decompression. The decrease in the main amide I frequency from 1627 to 1621 cm^{-1} characterizes the formation of optimal hydrogen bonds between the sheets.

The BAM images of the pure FP23 layer at increasing surface pressures from 3 to 30 mN/m (Fig. 2) display a progressive increase of the averaged normalized gray level during the compression and a homogeneisation of the surface. At the end of the compression (30 mN/m), it is possible to estimate the thickness of the layer using the BAM software and a refractive index of 1.50 for the FP23. Then, ≈13 Å is obtained for the layer of pure FP23 at 30 mN/m, which is in agreement with a monolayer of antiparallel β-sheets mainly flat oriented at the interface.

3.1.2. FP23 inserted into a lipid monolayer of DOPC/Cholesterol/DOPE/DOPG 6/5/3/2

PMIRRAS spectra of FP23 inserted into a lipid monolayer are registered after codeposition at the air/water interface of a FP23/lipid (DOPC/Chol/DOPE/DOPG 6/5/3/2*)* mixture at a defined lipid to peptide ratio, Ri. The spectra obtained (Fig. 3A and B) show lipid bands around 1730 cm^{-1} and 1460 cm^{-1}, respectively, due to ν (C═O) ester and δ (CH_2) of the acyl chains [53,54].

At Ri=50, i.e., the lowest peptide content used, the amide I band of FP23 remains centered around 1655 cm^{-1} whatever the lateral pressure from 10 to 30 mN/m, which is characteristic of an α-helicoidal structure of FP23. At 10 mN/m, no amide II band is shown around 1550 cm^{-1}, this means that the α-helix is oriented with its axis mainly parallel to the interface plane. When the pressure increases up to 30 mN/m, the amide II band appears and the amide I (1655 cm^{-1})/amide II (1550 cm^{-1}) ratio decreases which is characteristic of a progressive reorientation of the α-helix to a more tilted orientation (≈60°) with regard to the interface normal [50,51].

At Ri=10, i.e., higher peptide content, there is a modification of the amide I domain during the compression of the mixed monolayer. Indeed, at 10 mN/m, the

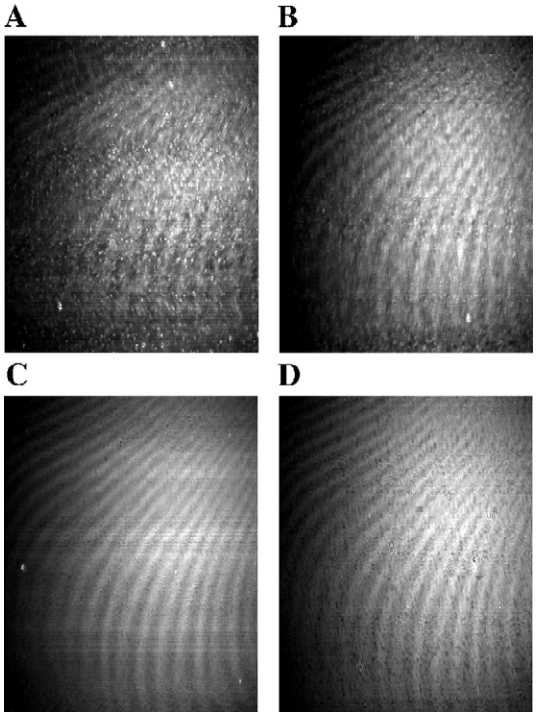

Fig. 2. Brewster angle microscopy images of FP23 alone at the air/water interface. A: 3 mN/m, GL=80, ET=1/50 s; B: 10 mN/m, GL=150, ET=1/50 s; C: 20 mN/m, GL=120, ET=1/120 s; D: 30 mN/m, GL=160, ET=1/120 s. Subphase: phosphate buffer 60 mM, NaCl 100 mM, pH=7.5–T=23 °C. GL=average gray level; ET=exposition time.

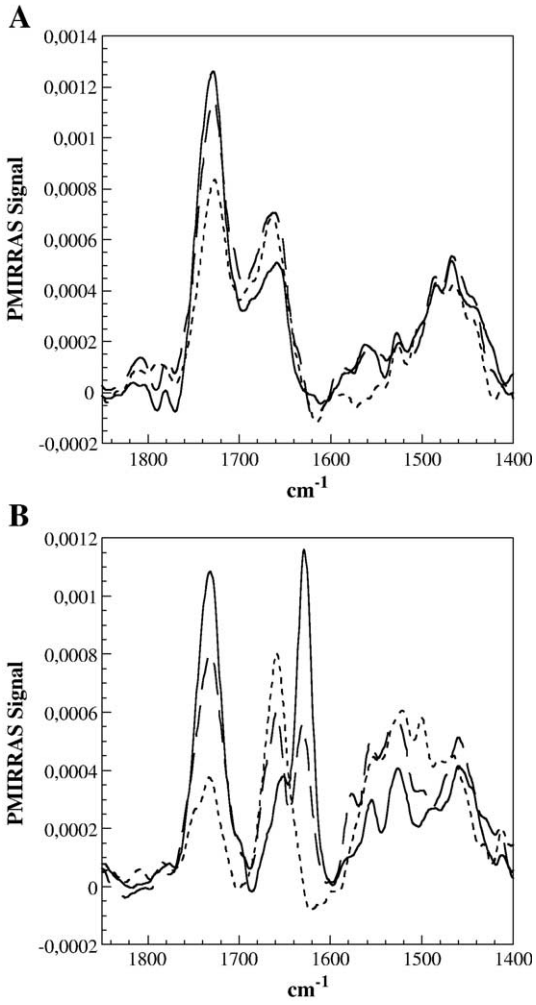

Fig. 3. PM-IRRAS spectra of FP23 inserted in a lipid monolayer of DOPC/Chol/DOPE/DOPS (6/5/3/2). A: Ri=50, - - - 10 mN/m, – – – 20 mN/m, —— 30 mN/m. B: Ri=10, - - - 10 mN/m, – – – 20 mN/m, —— 30 mN/m. Ri=[lipid] / [FP23], Subphase: phosphate buffer 60 mM, NaCl 100 mM, pH=7.5–T=23 °C.

amide I band is centered around 1655 cm^{-1} which is characteristic of an α-helix structure. The amide I (1655 cm^{-1})/amide II (1550 cm^{-1}) ratio of about 1.4 shows that that main axis of the α-helix is tilted form about 45° towards the normal to the interface. When pressure increases up to 30 mN/m, there is a progressive appearance of an amide I band around 1625 cm^{-1} which becomes predominant at 30 mN/m. Such a change is characteristic of a progressive structural transition from α-helix to β-sheets which is again irreversible under decompression (not shown). At 30 mN/m, the strong amide I (1625 cm^{-1})/amide I′ (1690 cm^{-1}) ratio indicates that the β-sheets are mainly flat oriented in the lipid interface plane.

The evolution of the morphology of a DOPC/chol/DOPE/DOPG (6/5/3/2) lipid monolayer in presence of FP23 was investigated by BAM (Fig. 4). The lipid monolayer alone (Fig. 4A) displays a quite homogeneous liquid phase whose luminosity increases in parallel with the compression. The few bright spots are characteristic of lipid aggregates. At 30 mN/m using the averaged gray level value and a refractive index of 1.46 for the pure lipid, the layer thickness is estimated to 22–23 Å with the BAM software. This is coherent with a fluid monolayer of mainly dioleyl (C18:1) lipid acyl chains. The presence of FP23 in the lipid monolayer at Ri=50 or Ri=10 strongly modifies the morphology of the monolayer. For Ri=50 (Fig. 4B), the averaged luminosity of the mixed FP23/lipid layer increases at 20 and 30 mN/m compared to the pure lipid monolayer due to bright small aggregated domains and ribbons. They are probably characteristic of lipid regions more concentrated in FP23. For Ri=10 (Fig. 4C), a phase transition occurs around 10 mN/m and bright filamentous domains and patches appear for higher lateral pressures. They are characteristic of high concentrations of FP23 which probably aggregates and condenses in the monolayer. The luminosity increase compared to the pure lipid monolayer is probably characteristic more of a refractive index increases at the interface consecutive to FP23 presence than of an important average thickness increase. Indeed, at 30 mN/m using the BAM software and an averaged refractive index of 1.48/1.49 for the mixed FP23/lipid layer (considering n=1.46 for pure lipid and n=1.50 for FP23), the thickness of the domains is estimated at 23–26 Å.

3.2. Polarized ATR study of the FP23 inserted into lipid bi- or multibi-layers

To investigate the behaviour of FP23 in lipid models closer to the natural membrane structure, polarized ATR experiments using multibilayers of the previous lipid mixture DOPC/Cholesterol/DOPE/DOPG (6/5/3/2) and a single bilayer of DMPC incorporating FP23 at different lipid to peptide ratios, Ri, were performed. It is then possible to analyze the structure and the orientation of the FP23 in such membrane models as well as the perturbations induced on the lipids.

3.2.1. FP23 structure

The ATR spectra presented in the 1800–1550 cm^{-1} domain (Figs. 5 and 6) show the ν (C═O) ester band of the lipid around 1735 cm^{-1} and the amide I region characteristic of the FP23 between 1600 and 1700 cm^{-1}. Whatever the lipid system (multibilayers of DOPC/Cholesterol/DOPE/DOPG or single bilayer of DMPC), the structural behaviour of FP23 is comparable at a defined lipid to peptide ratio. Indeed, when the FP23 is diluted in the lipids (Ri=200 in multibilayers and Ri=100 in the bilayer), the amide I region displays two bands (Figs. 5A and 6A, respectively): a component around 1655 cm^{-1} characteristic of an α-helix and a component around 1625 cm^{-1} (and 1685 cm^{-1} in Fig. 6A) characteristic of antiparallel β-sheets. The decomposition of the amide I domain and the correction of residual water contribution allow the estimation of 48% of α-helix/52% of β-sheets in

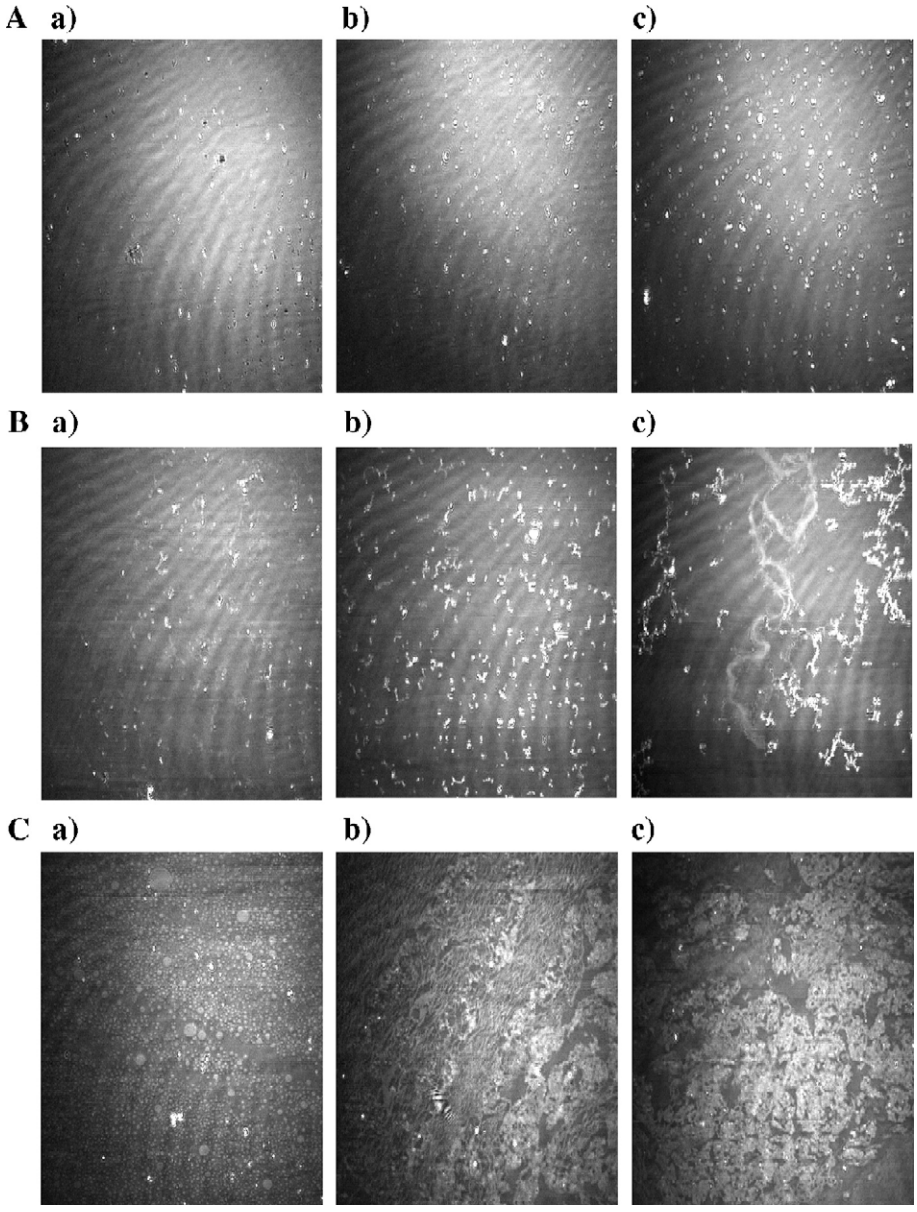

Fig. 4. Brewster angle microscopy images of FP23 inserted in a lipid monolayer (DOPC/Chol/DOPE/DOPG, 6/5/3/2). A: Lipid monolayer alone. (a) 10 mN/m, GL=80, ET=1/50 s; (b) 20 mN/m, GL=85, ET=1/50 s; (c) 30 mN/m, GL=100, ET=1/50 s. B: FP 23 inserted in the lipid monolayer, Ri=50. (a) 10 mN/m, GL=80, ET=1/50 s; (b) 20 mN/m, GL=110, ET=1/50 s; (c) 30 mN/m, GL=125, ET=1/50 s. C: FP 23 inserted in the lipid monolayer, Ri=10. (a) 10 mN/m, GL=90, ET=1/50 s; (b) 20 mN/m, GL=85, ET=1/120 s; (c) 30 mN/m, GL=135, ET=1/120 s. Subphase: phosphate buffer 60 mM, NaCl 100 mM, pH=7.5–T=23 °C. Ri=[lipid]/[FP23], GL=average gray level; ET=exposition time.

the multibilayer system and 42% of α-helix/54% of β-sheets in the single bilayer system. At high FP23 concentration in the lipids (Ri=50) there is mainly a well-defined amide I band around 1625 cm^{-1} with a weak contribution around 1685 cm^{-1} characteristic of a predominant structure of antiparallel β-sheets (Figs. 5B and 6B). For FP23 in the single bilayer system, the shoulder around 1655 cm^{-1} shows the presence of a residual α-helix structure (Fig. 6B). The decomposition of the amide I domain allows the estimation of approximately 80% and 75% of FP23 folded into β-sheets in the multibilayers and in the single bilayer, respectively.

3.2.2. FP23 orientation in the lipid systems

The polarized ATR spectra allow the evaluation of the dichroic ratio of the amide I band of α-helix at 1655 cm^{-1} and amide I and I′ of antiparallel β-sheets at 1625 cm^{-1} and 1685 cm^{-1}, respectively, for the diluted concentrations of FP23 in the lipid systems (Table 1). To explain these, data simulations were performed as described in Materials and methods. The evolution of the dichroic ratio of the α-helix versus the angle of the main axis with respect to the verticale of the interface (Fig. 7A) shows an orientation of 36.5±3.0° for the α-helix of FP23 in lipid multibilayers of DOPC/Chol/DOPE/DOPG at Ri=200 and 39.0±5.0° for

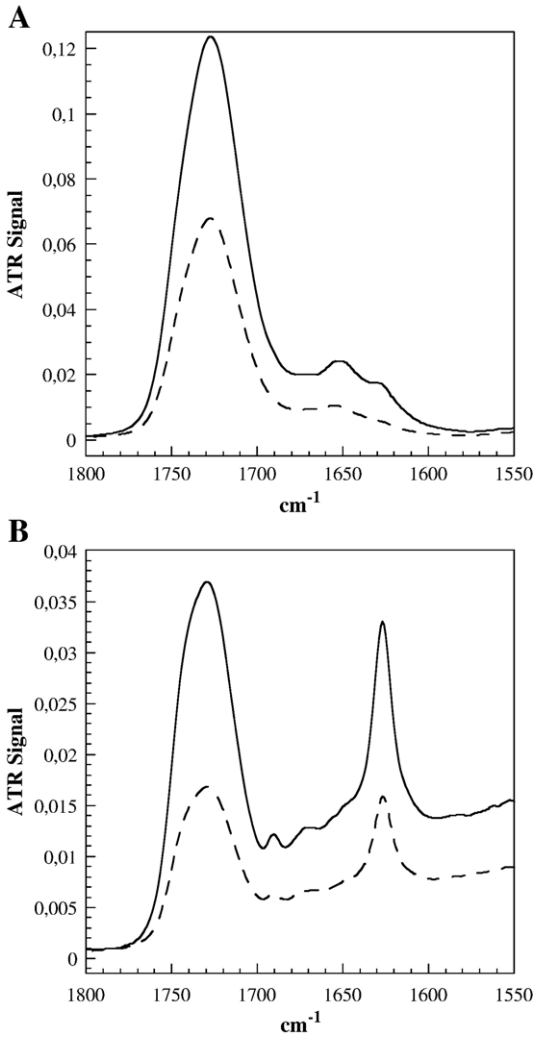

Fig. 5. ATR spectra on diamond crystal of FP 23 inserted into lipid multibilayers (DOPC/Chol/DOPE/DOPG, 6/5/3/2) hydrated by D_2O. A: Ri=200; B: Ri=50, —— P polarization, – – – S polarization.

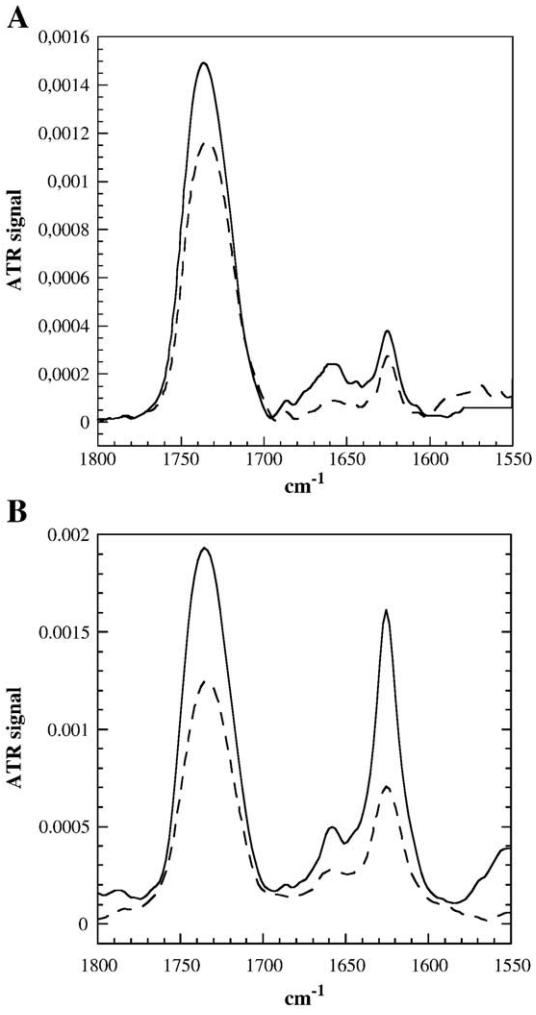

Fig. 6. ATR spectra on Ge crystal of FP 23 inserted into lipid bilayers of DMPC hydrated by D_2O. A: Ri=100 ; B: Ri=50, —— P polarization, – – – S polarization.

the α-helix of FP23 in lipid bilayer of DMPC at Ri=100. Concerning the antiparallel β-sheets, simulations which gave the closest results to the experimental data were obtained for variations of the tilt angle θ (rotation around u) of an initially flat oriented β-sheet, then only the results got for some (0, θ, 0) combinations are presented (Fig. 7B). Then, a tilt angle of 36.0±2.0° for the β-sheets of FP23 in lipid multibilayers of DOPC/Chol/DOPE/DOPG at Ri=200 and 30.0±2.0° for the β-sheets of FP23 in lipid bilayer of DMPC at Ri=100 were obtained.

No orientation was determined for the β-sheets obtained for the concentrated lipid to peptide ratio Ri=50 since perturbations on lipids were too important (see next paragraph).

3.2.3. Lipid chains perturbations

To evaluate the consequence of the FP23 insertion on the organization of the lipid chains in the multibilayers and in the bilayer, the evolution of the frequencies of the antisymmetric and symmetric stretching modes of methylene groups, $\nu_s(CH_2)$ and $\nu_{as}(CH_2)$, respectively, were measured at the various Ri tested (Table 2). Indeed, the frequencies of these bands are known to be sensitive to changes in the configuration of the acyl chains, in chain mobility and packing [55–58]. The $\nu_s(CH_2)$ and $\nu_{as}(CH_2)$

Table 1
Dichroic ratios (R_{ATR}) of the amide I band of FP23 diluted in a bilayer or multibilayers (Ri=[lipid]/[FP23])

	α-helix	Antiparallel β-sheet	
	R_{ATR} (1655 cm^{-1})	R_{ATR} (1625 cm^{-1})	R_{ATR} (1685 cm^{-1})
Multibilayers[a] Ri=200	2.45±0.1	2.10±0.1	0.60±0.1
Bilayer[b] Ri=100	1.80±0.1	1.30±0.1	0.90±0.1

[a] Composition of multibilayers: DOPC/Chol/DOPE/DOPG-6/5/3/2, ATR on diamond crystal.
[b] Composition of the bilayer: DMPC, ATR on germanium crystal.

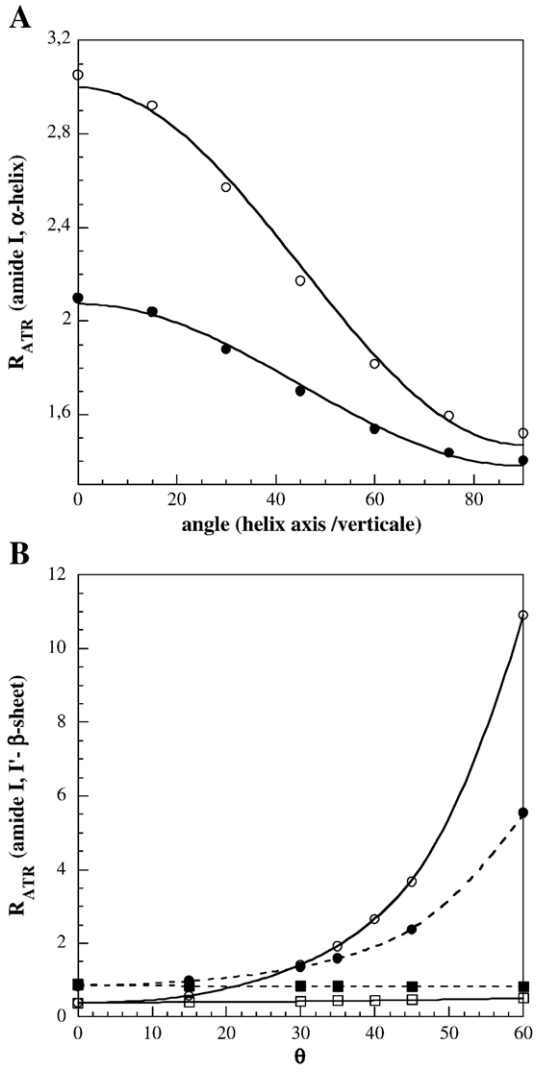

Fig. 7. Simulations of the evolution of the dichroic ratio, R_{ATR}, of the amide I bands of FP23. A: Simulations of the evolution of the dichroic ratio R_{ATR} of the α-helix amide I band (1655 cm^{-1}) versus orientation of the helix axis towards the normal of the lipid layer(s).—○—: FP23 inserted in multibilayers on diamond ATR crystal (Ri=200), —●—: FP23 inserted in a bilayer on germanium ATR crystal (Ri=100). B: Simulations of the evolution of the dichroic ratio R_{ATR} of the β-sheet amide I (1625 cm^{-1}) and amide I′ (1685 cm^{-1}) band versus θ angle (rotation around the chains axis of a β-sheet initially oriented parallely to the lipid layer plane). FP23 inserted in multibilayers on diamond ATR crystal (Ri=200): —○— R_{ATR} (1625 cm^{-1}); —□— R_{ATR} (1685 cm^{-1}). FP23 inserted in a bilayer on germanium ATR crystal (Ri=100):- - - ● - - - R_{ATR} (1625 cm^{-1}); - - - ■ - - - R_{ATR} (1685 cm^{-1}).

frequencies are higher for the multibilayer lipid system of DOPC/Cholesterol/DOPG/DOPE than for the bilayer of DMPC ($\nu_{as}(CH_2)$=2924.0 cm^{-1} for the multibilayers compared to $\nu_{as}(CH_2)$=2919.8 cm^{-1} for the bilayer and $\nu_s(CH_2)$=2853.5 cm^{-1} for the multibilayers compared to $\nu_s(CH_2)$=2850.6 cm^{-1} for the bilayer). This shows more disorder in the chains of the multibilayer system compared to the bilayer which can be explained by the coexistence of different nature of lipid chains. Indeed, the main phospholipids chains of the multibilayers are unsaturated dioleyl chains (C18:1) with negative temperatures of phase transition (−15 °C to −20 °C) while the bilayer is composed of saturated dimyristoyl chains (C14:0) with phase transition temperature around 23 °C. After FP23 insertion, even at low FP23 content (Ri=200 in the multibilayers and Ri=100 in the bilayer), there is an increase in the frequencies of the $\nu_s(CH_2)$ and $\nu_{as}(CH_2)$ whatever the lipid system (Table 2) which shows an increase of the chains disorder with formation of gauche conformers due to the FP23 insertion in the system. This behaviour is confirmed at higher FP23 content (Ri=50) and more pronounced in the bilayer system which was initially more well packed.

Table 2
Frequencies of the $\nu_s(CH_2)$ and $\nu_{as}(CH_2)$ bands of lipid chains in presence or absence of FP23 (Ri=[lipid]/[FP23])

Ri	$\nu_{as}(CH_2)$−cm^{-1}		$\nu_s(CH_2)$−cm^{-1}	
	Multibilayers[a]	Bilayer[b]	Multibilayers[a]	Bilayer[b]
∞ (no FP23)	2924.0	2919.8	2853.5	2850.6
200	2924.8	n.d.	2853.6	n.d.
100	n.d.	2921.3	n.d.	2851.8
50	2924.8	2921.9	2854.0	2852.8

n.d. not determined.
[a] Composition of multibilayers: DOPC/Chol/DOPE/DOPG-6/5/3/2, ATR on diamond crystal.
[b] Composition of the bilayer: DMPC, ATR on germanium crystal.

To go further in the analysis of the lipid chains perturbation induced by FP23 insertion, the dichroic ratio (R_{ATR}) of the $\nu_s(CH_2$-2853 cm^{-1}) band of lipid chains was measured on the polarized ATR spectra (Table 3). Indeed, since the transition moment for the $\nu_s(CH_2)$ lies perpendicular to the chain axis, the introduction of disorder (trough the formation of gauche conformers) alters the direction of the main chain with respect to the ATR crystal vertical axis then the dichroic ratio is expected to provide a sensitive and quantitative indicator of acyl chain order. To estimate the average C−C−C angle of the lipid carbon chains with the normal to the interface from the measured dichroic ratios (R_{ATR}), some simulations were performed

Table 3
Dichroic ratio (R_{ATR}) of the $\nu_s(CH_2$−2853 cm^{-1}) band of lipid chains in with or without FP23 (Ri=[lipid]/[FP23]) and average C−C−C angle (γ) of the lipid carbon chains with the normal to the interface

Ri	Multibilayers[a]		Bilayer[b]	
	R_{ATR} (2853 cm^{-1})	γ average C−C−C angle)°	R_{ATR} (2853 cm^{-1})	γ average C−C−C angle)°
∞ (no FP23)	1.40±0.06	43.8±1.0	1.23±0.04	39.0±2.5
200	1.44±0.06	44.8±2.0	n.d.	n.d.
100	n.d.	n.d.	1.28±0.04	41.4±2.0
50	1.93± 0.03	53.8±1.0	1.55±0.06	54.2±3.0

n.d. not determined.
[a] Composition of multibilayers: DOPC/Chol/DOPE/DOPG-6/5/3/2, ATR on diamond crystal.
[b] Composition of the bilayer: DMPC, ATR on germanium crystal.

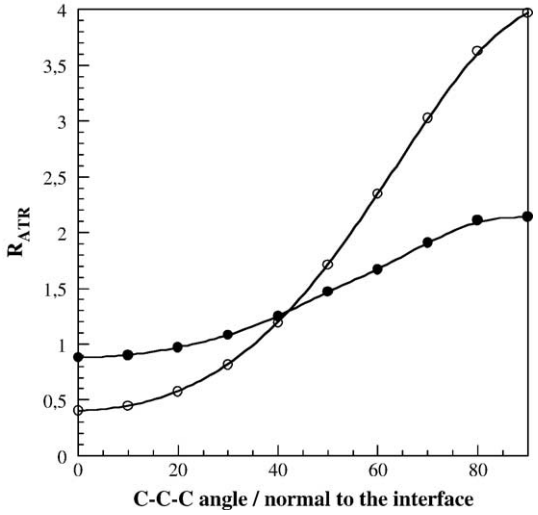

Fig. 8. Simulations of the evolution of the dichroic ratio R_{ATR} of ν (CH_2) band at 2853 cm^{-1} versus C–C–C angle of the acyl chains with respect to the normal to the interface. —○—: for multibilayers on diamond ATR crystal, —●—: for a bilayer on germanium ATR crystal.

(Fig. 8). The R_{ATR} values obtained for the lipids alone and the correspondent average C–C–C angles of the multibilayers and the bilayer, respectively, (Table 3) are in good agreement with the more fluid state of the multibilayer compared to the bilayer determined from the stretching frequencies of the methylene groups. When FP23 is inserted, there is an increase of R_{ATR} whatever the lipid system (Table 3) which corresponds to an increase of the average C–C–C angle of the lipid chains with the normal to the interface. This shows an increase of the number of gauche conformations then of disorder in the lipid chains due to FP23. At higher FP23 concentrations (Ri=50), the average C–C–C angles are closed to the "magic angle" (54.7°) which shows a quasi-isotropic organization of the lipid chains then a complete disorganization induced by the FP23.

4. Discussion

4.1. Structural polymorphism of FP23

The IR results of the present study show the structural polymorphism of the FP23 and its ability to transit quasi-irreversibly (during the time scale of observation) from an α-helix to antiparallel β-sheets. Such a transition occurs for the peptide alone at the air/water interface due to lateral pressure increase as well as for the peptide inserted in various lipid systems: mono, bi and multibilayers. In the lipid systems used, the transition occurs at different lipid to peptide ratios, Ri, whether the structure of the lipid membrane model. In the lipid monolayer, the structural transition is induced by compression at high FP23 concentration (Ri=10) while when FP23 is more diluted in the monolayer (Ri=50) the α-helix remains predominant whatever the lateral pressure. The behaviour is different in bilayer systems. Indeed, even at diluted FP23 concentrations (Ri=200 in multibilayers and Ri=100 in a single bilayer), there is coexistence of both structures in quasi equal proportions while antiparallel β-sheets are the predominant structure at more concentrated FP23 concentrations (Ri=50) (Table 4). Such an ability of the FP23 (or of a shorter sequence of 16 residues) to exist as an α-helix or as β-sheets or to transit from an α-helix to antiparallel β-sheets was previously demonstrated [9,11–14,18,20,23,26,28–30,32,34,59,60] but the exact conditions and physicochemical parameters which modulate this structural behaviour remain unclear.

In the present work, the structure of the membrane model (monolayer or (multi)bilayers) seems to influence the Ri at which the structural transition occurs but the lipid composition of the membrane model does not seem to be a critical parameter conversely to what was suggested by some previous studies [9,28,29]. Indeed, the structural behaviours of FP23 in a single bilayer of zwitterionic DMPC and in multibilayers of a weakly negatively charged

Table 4
Summary of the structure and orientations of FP23 in the various experimental conditions used (Ri=[lipid]/[FP23])

Experimental conditions	Ri	Secondary structure	Orientation
FP23 alone at the air/water interface	–	Transition from α-helix to β-sheets induced by compression	α-helix: ≈60°/interface normal
			β-sheets: mainly flat oriented
FP23 inserted into a monolayer of DOPC/Cholesterol/DOPE/DOPG (6/5/3/2)	50	α-helix	Reorientation induced by compression from parallel to the interface to ≈60°/interface normal
	10	Transition from α-helix to β-sheets induced by compression	α-helix: ≈45°/interface normal
			β-sheets: mainly flat oriented
FP23 inserted into multibilayers of DOPC/Cholesterol/DOPE/DOPG (6/5/3/2)	200	α-helix (48%)	α-helix: 36.5±3.0°/interface normal
		β-sheets (52%)	β-sheets: tilt angle of 36.0±2.0°
	50	β-sheets (>80%)	n.d.
FP23 inserted into a single bilayer of DMPC	100	α-helix (42%)	α-helix: 39.0±5.0°/interface normal
		β-sheets (54%)	β-sheets: tilt angle of 30.0±2.0°
	50	β-sheets (>75%)	n.d.

n.d.: not determined due to very important lipid disorder induced by FP23 in (multi)bilayers.

mixture of DOPC/Cholesterol/DOPE/DOPG (6/5/3/2) are comparable.

The formation of antiparallel β-sheets of FP23 is probably consecutive to an oligomerization of the fusion peptide in the membrane. Such an accumulation of FP23 in membrane may have biological significance. Indeed, formation of fusion oligomers was suggested to be linked to fusion activity for both envelope protein-mediated fusion and for liposome fusion mediated by fusion peptides [8,19,28,29]. For instance, in the case of the fusion peptide of the Sendaï virus [61], the peptide could self-assemble in its membrane-bound state, thus suggesting its role in assisting the assembly of the envelope protein of the virus.

Then, up to now, the exact nature of the fusogenic structure of FP23 is still uncertain and this could be this conformational polymorphism which may be physiologically relevant for fusogenic activity. Indeed, conformational flexibility has been shown to be a significant factor that differentiates active and inactive FPs [27]. It is also hypothesized that conformational polymorphism might contribute to the flexibility of the fusogenic complex during the fusion cycle [4,35,62]. Some studies suggest that the conversion of an α-helical structure to the more extended β-conformation plays an important role during membrane fusion to allow access of the fusion peptide to the trans-monolayer of the target membrane [63]. For others adoption of two conformations might also be related to induction of important membrane perturbations which could facilitate fusion process [35]. It is also possible that there is a transient fusogenic structure that is unstructured or flexible rather than a well-defined α-helical or β-strand conformation which is responsible for fusion [31,64].

4.2. Tilted orientation of FP23 in membrane models and consequences on lipid organization

The present study is one of the first which so carefully investigate the orientation of FP23 alone and in membrane models close to the natural conditions (structure, composition and hydration level). Indeed, we demonstrate experimentally that the FP23 displays an ability to adopt a tilted orientation in the lipid model membrane used (Table 4) but the orientation is different whether the structure of the lipid system, monolayer or (multi)bilayers. Indeed, concerning the FP23 alone or inserted into a lipid monolayer, the orientation of the α-helix remains relatively weakly tilted with respect to the interface normal (≈60° for the α-helix of FP23 alone and inserted into the compressed lipid monolayer at Ri=40 and ≈45° at Ri=10 and low surface pressure) compared to the orientations obtained for the same structure in (multi)bilayers for instance (36.5±3.0° for the α-helix of FP23 in multibilayers at Ri=200 and 39.0±5.0° for the α-helix of FP23 in a single bilayer). Such a difference may be due to the fact that a lipid monolayer does not match correctly the hydrophobic thickness of a membrane and does not allow a proper orientation of FP23 which is then too long to match the hydrophobic part of the lipids. Therefore, even if the monolayer system allows the detection of the ability of FP23 to adopt a tilted orientation, the lipid (multi)bilayers seem to be more relevant models to fit the biological membrane and the orientation of FP23 in such systems will be more representative of the reality.

Then, in multibi- or single bilayer systems whatever their composition, the orientational results obtained at the diluted FP23 ratios (Ri=200 and 100 respectively) are highly comparable. Indeed, the α-helix is strongly tilted with regard to the interface normal (38° in average) while the β-sheet part is more weakly tilted (tilt angle of 33° in average) (Table 4) but both structures are inserted with a tilt angle in the lipid systems. Such results are in good agreement with the computer simulations of interaction of viral fusion peptides with host-cell membranes which first led to the hypothesis that the helices of fusogenic peptides are obliquely oriented with respect to the lipid water interface [65] and with the demonstration using ATR FTIR spectroscopy that a short portion (16 residues, FP16) of the fusion peptide of HIV is obliquely oriented in its membrane-bound state [12]. Recently, molecular dynamic simulations [66,67] and Monte-Carlo simulations [68] also conclude to an oblique orientation of an α-helix of the FP peptide from HIV 1 (44±6° for a FP16 and 38° for FP23 respectively). Further support for this oblique orientation comes from a study showing that the fusion peptide of the Sendai virus is obliquely oriented in its membrane bound state [61]. An oblique orientation was also documented for fusion peptides of protein like fertilin, a protein active in sperm–egg fusion [69] or other viruses like Ebola [70], SIV [71–73] or influenza [74] for instance.

Such an oblique orientation was postulated to locally disorganize the structure of the lipid bilayer and to generate new lipid phases that are thought to be associated with initial steps of membrane fusion by increasing the negative curvature strain, favoring the formation of inverted phases [12]. This hypothesis is in good agreement with the lipid chain disorder induced by the interaction of FP23 in (multi)bilayers as determined herein by polarized ATR spectroscopy. Indeed, we demonstrate an increase of the average C–C–C angle of the acyl chains (up to 2.5° in the bilayer) then of the gauche conformations number in the lipid chains even at diluted FP23 concentration in the lipids (Ri=200 in multibilayers and Ri=100 in a single bilayer). At higher FP23 concentration (Ri=50), a total lipid disorganization was measured due to the accumulation of antiparallel β-sheets in the model membrane.

To conclude, the present study confirms the structural polymorphism of HIV 1 fusion peptide FP23 and demonstrate its ability to transit quasi irreversibly (at the time scale of observation) from an α-helix to probably oligomerized antiparallel β-sheets. But further experiments are required to identify the nature of the fusogenic structure of FP23, if the secondary structure of the fusion

domain plays a role in affecting the fusogenic activity of the fusion peptide. Indeed, no answer can be given to this question up to now and the conformational flexibility of FP23 might play a crucial role in FP23 fusogenic activity. Our results clearly demonstrate a tilted orientation of the FP23 structures in (multi)bilayer model membranes closed to the natural conditions of structure, composition and hydration level and reinforce the hypothesis that an oblique orientation is determinant for fusogenic peptides since it could lead to lipid membrane perturbations favoring the initial steps of fusion. To go further and to assess if the structure and orientation of the isolated FP23 peptide bears any relevance to that of the peptide in the virus, studies are planned to carefully investigate the structural and orientational behaviour of a longer segment of FP peptide (FP33) as well as the FP+ ectodomain part of the gp41 protein by the performing IR techniques and spectral simulations used herein.

References

[1] F.D. Veronese, A.L. DeVico, T.D. Copeland, S. Oroszlan, R.C. Gallo, M.G. Sarngadharan, Characterization of gp41 as the transmembrane protein coded by the HTLV/LAV envelope gene, Science 229 (1985) 1402–1405.

[2] L.D. Hernandez, L.R. Hoffman, T.G. Wolfsberg, J.M. White, Virus–cell and cell–cell fusion, Annu. Rev. Cell Dev. Biol. 12 (1996) 627–661.

[3] D.S. Dimitrov, Cell biology of virus entry, Cell 101 (2000) 697–702.

[4] D.M. Eckert, P.S. Kim, Mechanisms of viral membrane fusion and its inhibition, Annu. Rev. Biochem. 70 (2001) 777–810.

[5] R. Blumenthal, M.J. Clague, S.R. Durell, R.M. Epand, Membrane fusion, Chem. Rev. 103 (2003) 53–69.

[6] D.C. Chan, D. Fass, J.M. Berger, P.S. Kim, Core structure of gp41 from the HIV envelope glycoprotein, Cell 89 (1997) 263–273.

[7] E.O. Freed, D.J. Myers, R. Risser, Characterization of the fusion domain of the human immunodeficiency virus type 1 envelope glycoprotein gp41, Proc. Natl. Acad. Sci. U. S. A. 87 (1990) 4650–4654.

[8] E.O. Freed, E.L. Delwart, G.L. Buchschacher Jr., A.T. Panganiban, A mutation in the human immunodeficiency virus type 1 transmembrane glycoprotein gp41 dominantly interferes with fusion and infectivity, Proc. Natl. Acad. Sci. U. S. A. 89 (1992) 70–74.

[9] M. Rafalsky, J.D. Lear, W.F. De Grado, Phospholipid interactions of the synthetic peptides representing the N-terminus of HIV gp41, Biochemistry 29 (1990) 7917–7922.

[10] V.A. Slepushkin, S.M. Andreev, M.V. Sidorova, G.B. Melikyan, V.B. Grigoriev, V.M. Chumakov, A.E. Grinfeldt, R.A. Manukyan, E.V. Karamov, Investigation of human immunodeficiency virus fusion peptides. Analysis of interrelations between their structure and function, AIDS Res. Hum. Retrovir. 8 (1992) 9–18.

[11] I. Martin, F. Defrise-Quertain, E. Decroly, M. Vandenbranden, R. Brasseur, J.M. Ruysschaert, Orientation and structure of the NH2-terminal HIV-1 gp41 peptide in fused and aggregated liposomes, Biochim. Biophys. Acta 1145 (1993) 124–133.

[12] I. Martin, H. Schaal, A. Scheid, J.M. Ruysschaert, Lipid membrane fusion induced by the human immunodeficiency virus type I gp41 N-terminal extremity is determined by its orientation in the lipid bilayer, J. Virol. 70 (1996) 298–304.

[13] J.L. Nieva, S. Nir, A. Muga, F.M. Goni, J. Wilschut, Interaction of the HIV-1 fusion peptide with phospholipid vesicles: different structural requirements for fusion and leakage, Biochemistry 33 (1994) 3201–3209.

[14] J.L. Nieva, S. Nir, J. Wilschut, Destabilization and fusion of zwitterionic large unilamellar lipid vesicles induced by a beta-type structure of the HIV-1 fusion peptide, J. Liposome Res. 8 (1998) 165–182.

[15] P.W. Mobley, H.F. Lee, C.C. Curtain, A. Kirkpatrick, A.J. Waring, L.M. Gordon, The amino-terminal peptide of HIV-1 glycoprotein 41 fuses human erythrocytes, Biochim. Biophys. Acta 1271 (1995) 304–314.

[16] H. Schaal, M. Klein, P. Gehrmann, O. Adams, A. Scheid, Requirement of N-terminal amino acid residues of gp41 for human immunodeficiency virus type 1-mediated cell fusion, J. Virol. 69 (1995) 3308–3314.

[17] M.D. Delahunty, I. Rhee, E.O. Freed, J.S. Bonifacino, Mutational analysis of the fusion peptide of the human immunodeficiency virus type 1: identification of critical glycine residues, Virology 218 (1996) 94–102.

[18] S.R. Durell, I. Martin, J.M. Ruysschaert, Y. Shai, R. Blumenthal, What studies of fusion peptides tell us about viral envelope glycoprotein-mediated membrane fusion (review), Mol. Membr. Biol. 14 (1997) 97–112.

[19] Y. Kliger, A. Aharoni, D. Rapaport, P. Jones, R. Blumenthal, Y. Shai, Fusion peptides derived from the HIV type 1 glycoprotein 41 associate within phospholipid membranes and inhibit cell–cell fusion. Structure–function study, J. Biol. Chem. 272 (1997) 13496–13505.

[20] F.B. Pereira, F.M. Goni, A. Muga, J.L. Nieva, Permeabilization and fusion of uncharged lipid vesicles induced by the HIV-1 fusion peptide adopting an extended conformation: dose and sequence effects, Biophys. J. 73 (1997) 1977–1986.

[21] E. Pecheur, J. Sainte-Marie, A. Bienvenue, D. Hoekstra, Peptides and membrane fusion: towards an understanding of the molecular mechanism of protein-induced fusion, J. Membr. Biol. 167 (1999) 1–17.

[22] M. Pritsker, J. Rucker, T.L. Hoffman, R.W. Doms, Y. Shai, Effect of nonpolar substitutions of the conserved Phe11 in the fusion peptide of HIV-1 gp41 on its function, structure, and organization in membranes, Biochemistry 38 (1999) 11359–11371.

[23] L.M. Gordon, C.C. Curtain, Y.C. Zhong, A. Kirkpatrick, P.W. Mobley, A.J. Waring, The amino-terminal peptide of HIV-1 glycoprotein 41 interacts with human erythrocytes membranes: peptide conformation, orientation and aggregation, Biochim. Biophys. Acta 1139 (1992) 257–272.

[24] D.K. Chang, W.J. Chien, S.F. Cheng, The FLG motif in the N-terminal region of glucoprotein 41 of human immunodeficiency virus type 1 adopts a type-I beta turn in aqueous solution and serves as the initiation site for helix formation, Eur. J. Biochem. 247 (1997) 896–905.

[25] A.J. Waring, P.W. Mobley, L.M. Gordon, Conformational mapping of a viral fusion peptide in structure-promoting solvents using circular dichroism and electrospray mass spectrometry, Proteins 2 (1998) 38–49.

[26] D.K. Chang, S.F. Cheng, W.J. Chien, The amino-terminal fusion domain of the human immunodeficiency virus type I gp41 inserts into the SDS micelle primarily as α helix with a conserved glycine at the micelle–water interface, J. Virol. 71 (1997) 6593–6602.

[27] K.F. Morris, X. Gao, T.C. Wong, The interactions of the HIV gp41 fusion peptides with zwitterionic membrane mimics determined by NMR spectroscopy, Biochim. Biophys. Acta 1667 (2004) 67–81.

[28] J. Yang, P.D. Parkanzky, B.A. Khunte, C.G. Canlas, R. Yang, C.M. Gabrys, D.P. Weliky, Solid state NMR measurements of conformation and conformational distributions in the membrane-bound HIV-1 fusion peptide, J. Mol. Graph. Model. 19 (2001) 129–135.

[29] J. Yang, M. Gabrys, D.P. Weliky, Solid-state NMR evidence for an extended βstrand conformation of the membrane bound HIV-1 fusion peptide, Biochemistry 40 (2001) 8126–8137.

[30] J. Yang, D.P. Weliky, Solid-state nuclear magnetic resonance evidence for parallel and antiparallel strand arrangements in the membrane-associated HIV-1 fusion peptide, Biochemistry 42 (2003) 11879–11890.

[31] J. Yang, M. Prorok, F.J. Castellino, D.P. Weliky, Oligomeric β-

structure of the membrane bound HIV-1 fusion peptide formed from soluble monomers, Biophys. J. 87 (2004) 1951–1963.
[32] C. Curtain, F. Separovic, K. Nielsen, D. Craik, Y. Zhong, A. Kirkpatrick, The interactions of the N-terminal fusogenic peptide of HIV-1 gp41 with neutral phospholipids, Eur. Biophys. J. 28 (1999) 427–436.
[33] S.G. Peisajovich, R.Q. Epand, M. Pritsker, Y. Shai, R.M. Epand, The polar region consecutive to the HIV fusion peptide participates in membrane fusion, Biochemistry 39 (2000) 1826–1833.
[34] P.W. Mobley, A.J. Waring, M.A. Sherman, L.M. Gordon, Membrane interactions of the synthetic N-terminal peptide of HIV-1 gp41 and its structural analogs, Biochim. Biophys. Acta 1418 (1999) 1–18.
[35] A. Saez-Cirion, J.L. Nieva, Conformational transitions of membrane-bound HIV-1 fusion peptide, Biochim. Biophys. Acta 1564 (2002) 57–65.
[36] D. Blaudez, T. Buffeteau, J.C. Cornut, B. Desbat, N. Escafre, M. Pezolet, J.M. Turlet, Polarization modulation IRFT spectroscopy at the air–water interface, Thin Solid Films 242 (1994) 146–150.
[37] E. Goormaghtigh, V. Cabiaux, J.M. Ruysschaert, Secondary structure and dosage of soluble and membrane proteins by attenuated total reflection Fourier transform infra-red spectroscopy on hydrated films, Eur. J. Biochem. 193 (1990) 409–420.
[38] E. Goormaghtigh, V. Cabiaux, J.M. Ruysschaert, Determination of soluble and membrane protein structure by Fourier Transform Infrared spectroscopy, in: H.J. Hilderson, G.B. Ralston (Eds.), Subcellular Biochemistry, Physicochemical Methods in the Study of Biomembranes, vol. 23, Plenum Press, New York, 1994, pp. 329–450.
[39] E. Goormaghtigh, V. Raussens, J.M. Ruysschaert, Attenuated total reflection infrared spectroscopy of proteins and lipids in biological membranes, Biochim. Biophys. Acta 1422 (1999) 105–185.
[40] T. Buffeteau, D. Blaudez, E. Péré, B. Desbat, Optical constant determination in the infrared of the uniaxially oriented monolayers from transmittance and reflectance measurements, J. Phys. Chem., B 103 (1999) 5020–5027.
[41] F. Abeles, M.L. Théye, Méthode de calcul des constantes optiques des couches minces absorbantes à partir de mesures de réflexion et de transmission, Surf. Sci. 5 (1966) 325–331.
[42] J.D. Graybeal, Molecular Spectroscopy, Mac Graw Hill, Inc., New York, 1988, p. 665.
[43] T. Miyazawa, Molecular Vibrations and Structures of High Polymers: I. General Method of Normal Coordinate Treatment by Internal Coordinates and Infrared Frequencies and Conformations of (—CH_2—)n, (—CH_2O—)n, and (—CH_2OCH_2—)n, J. Chem. Phys. 35 (1961) 693–713.
[44] T. Miyazawa, in: G.D. Fasman, M. Dekker (Eds.), Poly-α Amino Acids, Chapter 2, New York, 1967, pp. 69–103.
[45] T. Buffeteau, E. Le Calvez, S. Castano, B. Desbat, D. Blaudez, J. Dufourcq, Anisotropic optical constants of α-helix and β-sheet secondary structures in the infrared, J. Phys. Chem., B 104 (2000) 4537–4544.
[46] T. Miyazawa, E.R. Blout, The infrared spectra of polypeptides in various conformations: amide I and II bands, J. Am. Chem. Soc. 83 (1961) 712–719.
[47] W.H. Moore, S. Krimms, Vibrational analysis of peptides, polypeptides, and proteins: II. β-Poly(L-alanine) and βpoly(L-alanylglycine), Biopolymers 5 (1976) 2465–2483.
[48] P.I. Haris, D. Chapman, Does Fourier-transform infrared spectroscopy provide useful information on protein structure? TIBS 17 (1992) 328–333.
[49] W.K. Surewicz, H.H. Mantsch, D. Chapman, Determination of protein secondary structure by Fourier transform infrared spectroscopy: a critical assessment, Biochemistry 32 (1993) 389–394.
[50] I. Cornut, B. Desbat, J.M. Turlet, J. Dufourcq, In situ study by polarization modulated Fourier transform infrared spectroscopy of the structure and orientation of lipids and amphipathic peptides at the air/water interface, Biophys. J. 70 (1996) 305–312.
[51] S. Castano, B. Desbat, M. Laguerre, J. Dufourcq, Structure, orientation and affinity for interfaces and lipids of ideally amphipathic lytic L_iK_j(i=2j) peptides, Biochim. Biophys. Acta 1416 (1999) 176–194.
[52] S. Castano, B. Desbat, J. Dufourcq, Ideally amphipathic β-sheeted peptides at interfaces: structure, orientation, affinities for lipids and hemolytic activity of $(KL)_mK$ peptides, Biochim. Biophys. Acta 1463 (2000) 65–80.
[53] G. Socrates, Infrared Characteristic Group Frequencies, John Wiley and Sons, New York, 1980.
[54] H.H. Mantsch, R.N. Mc Elhaney, Phospholipid phase transitions in model and biological membranes as studied by infrared spectroscopy, Chem. Phys. Lipids 57 (1991) 213–226.
[55] I.M. Asher, I.W. Levin, Effects of temperature and molecular interactions on the vibrational infrared spectra of phospholipid vesicles, Biochim. Biophys. Acta 468 (1977) 63–72.
[56] D.G. Cameron, H.L. Casal, H.H. Mantsch, Characterization of the pretransition in 1,2-dipalmitoyl-*sn*-glycero-3-phosphocholine by Fourier transform infrared spectroscopy, Biochemistry 19 (1980) 3665–3672.
[57] M.W. Rooney, Y. Lange, J.W. Kauffman, Acyl chain organization and protein secondary structure in cholesterol-modified erythrocyte membranes, J. Biol. Chem. 259 (1984) 8281–8285.
[58] J.W. Brauner, R. Mendelsohn, F.G. Prendergast, Attenuated total reflectance Fourier transform infrared studies of the interaction of melittin, two fragments of melittin, and (hemolysin with phosphatidylcholines, Biochemistry 26 (1987) 8151–8158.
[59] L.M. Gordon, P.W. Mobley, R. Pilpa, M.A. Sherman, A.J. Waring, Conformational mapping of the N-terminal peptide of HIV-1 gp41 in membrane environments using 13C-enhanced Fourier transform infrared spectroscopy, Biochim. Biophys. Acta 1559 (2002) 96–120.
[60] M.L. Bodner, C.M. Gabrys, P.D. Parkanzky, J. Yang, C.A. Duskin, D.P. Weliky, Temperature dependence and resonance assignment of 13C NMR spectra of selectively and uniformly labeled fusion peptides associated with membranes, Magn. Reson. Chem. 42 (2004) 187–194.
[61] D. Rapaport, Y. Shai, Interaction of fluorescently labeled analogues of the amino-terminal fusion peptide of Sendai virus with phospholipid membranes, J. Biol. Chem. 26 (1994) 15124–15131.
[62] R.W. Doms, J.P. Moore, HIV-1 membrane fusion: targets of opportunity, J. Cell Biol. 151 (2000) F9–F14.
[63] R.M. Epand, Lipid polymorphism and protein–lipid interactions, Biochim. Biophys. Acta 1376 (1998) 353–368.
[64] S. Afonin, R.W. Glaser, M. Berditchevskaia, P. Wadhwani, K.H. Guhrs, U. Mollmann, A. Perner, A.S. Ulrich, 4-Fluorophenylglycine as a label for 19F NMR structure analysis of membrane-associated peptides, ChemBioChem 4 (2003) 1151–1163.
[65] R. Brasseur, M. Vandenbranden, B. Cornet, A. Burny, J.M. Ruysschaert, Orientation into the lipid bilayer of an asymmetric amphipathic helical peptide located at the N-terminus of viral fusion proteins, Biochim. Biophys. Acta 1029 (1990) 267–273.
[66] S. Karnath, T.C. Wong, Membrane structure of the human immunodeficiency virus gp41 fusion domain by molecular dynamics simulation, Biophys. J. 83 (2002) 135–143.
[67] T.C. Wong, Membrane structure of the human immunodeficiency virus gp41 fusion peptide by molecular dynamics simulation: II. Glycine mutants, Biochim. Biophys. Acta 1609 (2003) 45–54.
[68] M.W. Maddox, M.L. Longo, Conformational partitioning of the fusion peptide of HIV-1 gp41 and its structural analogs in bilayer membranes, Biophys. J. 83 (2002) 3088–3096.
[69] I. Martin, R.M. Epand, J.M. Ruysschaert, Structural properties of the putative fusion peptide of fertilin, a protein active in sperm–egg fusion, upon interaction with the lipid bilayer, Biochemistry 37 (1998) 17030–17039.
[70] B. Adam, L. Lins, V. Stroobant, A. Thomas, R. Brasseur, Distribution of hydrophobic residues is crucial for the fusogenic properties of the Ebola virus GP2 fusion peptide, J. Virol. 78 (2004) 2131–2136.
[71] A. Colotto, I. Martin, J.M. Ruysschaert, A. Sen, S.W. Hui, R.M. Epand, Structural study of the interaction between the SIV

fusion peptide and model membranes, Biochemistry 35 (1996) 980–989.
[72] A. Schanck, J. Peuvot, R. Brasseur, Influence of the mode of insertion of SIV peptides into membranes on the structure of model membrane as studied by 31P NMR, Biochem. Biophys. Res. Commun. 250 (1998) 12–14.
[73] J.P. Bradshaw, M.J. Darkes, T.A. Harroun, J. Katsaras, R.M. Epand, Oblique membrane insertion of viral fusion peptide probed by neutron diffraction, Biochemistry 39 (2000) 6581–6585.
[74] J. Luneberg, I. Martin, F. Nussler, J.M. Ruysschaert, A. Herrmann, Structure and topology of the influenza virus fusion peptide in lipid bilayers, J. Biol. Chem. 270 (1995) 27606–27614.